



## Tip-assisted Si nanowire MOSFET aptasensor for cardiac biomarker detection

Anna Lukyanenko<sup>a,\*</sup>, Lev Shanidze<sup>a</sup>, Vasilisa Krasitskaya<sup>b</sup>, Olga Vshivkova<sup>c</sup>, Ludmila Frank<sup>b</sup>, Anton Tarasov<sup>a</sup>

<sup>a</sup> Kirensky Institute of Physics, Krasnoyarsk Scientific Center, Siberian Branch, Russian Academy of Sciences, Akademgorodok 50, bld. 38, Krasnoyarsk 660036, Russia

<sup>b</sup> Institute of Biophysics, Krasnoyarsk Scientific Center, Siberian Branch, Russian Academy of Sciences, Akademgorodok 50, bld. 50, Krasnoyarsk 660036, Russia

<sup>c</sup> Krasnoyarsk Scientific Center, Siberian Branch, Russian Academy of Sciences, Akademgorodok 50, Krasnoyarsk 660036, Russia

### ARTICLE INFO

#### Keywords:

Silicon nanowire field-effect transistor (Si-NW FET)  
AFM  
DNA aptamer  
Aptasensor  
Heart-type fatty acid-binding protein (hFABP)  
Biosensor  
Surface modification

### ABSTRACT

Miniature electronic sensors manufactured using modern silicon technology have been intensively studied as candidates for replacing chemical and biological test systems used in medicine for precision detection of proteins and molecules in liquids and gases. Selective recognition of low concentrations of biomarkers will make it possible to diagnose dangerous diseases at early stages, thereby ensuring their successful treatment. In this study, a method for electrical detection of a heart-type fatty acid-binding protein (hFABP) in air is proposed. To enhance the selectivity, silicon nanowire field-effect transistors (Si-NW FETs) with channel widths of 0.4, 1, and 3  $\mu\text{m}$  have been fabricated and pre-functionalized with an anti-hFABP DNA aptamer (FABPp1c-t38). It has been found that the FABPp1c-t38 and hFABP protein induce opposite shifts of threshold voltage  $V_{\text{th}}$  of the Si-NW FET. For a detected target, the voltage  $V_{\text{th}}$  shifts from +0.2 to +2.8 V. It has been established that the voltage  $V_{\text{th}}$  is a better signal as compared with other electrical characteristics of the transistor. This has allowed the hFABP detection at concentrations of 1 pM in a model buffer system. It is expected that the proposed cardiac target sensors and method for detection under dry conditions will contribute to the development and production of various electronic devices for application in medicine and other fields.

### 1. Introduction

Silicon is a key element of the modern micro- and nanoelectronic industry and silicon technology serves as a reliable platform for the development of new devices for application in various fields. The MOSFETs (metal–oxide–semiconductor field-effect transistor) has proven itself since the 70s of the last century, when pioneer works on the use of silicon FETs for sensing in liquid media were published [1]. In addition to their use in converters, low-power memory, and logic chips [2], MOSFETs find widespread usage in biosensing applications [3]. The nanoscale forms of silicon, including nanoribbons (NRs) and nanowires (NWs), have found wide application in electronic sensing platforms (ESPs) for selective detection of chemical and biological species [4]. The functional devices from bottom-up Si-NWs less than 10 nm in diameter have exhibited the remarkable sensitivity, but poor reproducibility. To date, there has been a lack of a reliable and commercially viable technological platform with devices fabricated using the bottom-up approach [5,6]. The top-down NWs or NRs FETs are highly

compatible with the state-of-the-art technology and can be produced in large volumes on one wafer by lithography, deposition, and etching. The obvious advantages of nanosensors, including their increased packaging density and ease of integration with lab-on-a-chip (LoC) techniques, are highly important for the development of next-generation sensor devices.

In this work, a device with a simple design is used, which requires neither alloying nor subsequent high-temperature annealing. In our work, we used a simple design of a MOSFET with Si-NWs, which requires fewer manufacturing processes and is therefore more economical. From the perspective of versatility, an open design for the current channel is convenient and a large number of receptors can be placed on its surface. This can be useful for various target sizes, from proteins to potentially organelles and cells, and avoids the steric effect [7]. According to the analytical results [8], the tunnel field-effect transistor (TFET) has been shown to be more energy-efficient and provide higher sensitivity due to its steeper subthreshold slope. However, it will be challenging to implement an aptasensor based on the TFET design that includes cavities. Nevertheless, simulations [9,10] have shown that for certain types

\* Corresponding author.

E-mail address: [lav@iph.krasn.ru](mailto:lav@iph.krasn.ru) (A. Lukyanenko).

of molecules, the TFET can be utilized in biosensor applications. The low levels of Si doping are valuable for sensing applications, since the sensitivity of a device increases with decreasing dopant concentration [4,11]. Si-NW FETs are ambipolar NW devices with Schottky barriers that serve as source (S) and drain (D) contacts. Schwalke et al. proposed a design of universal tunable NW transistors for the development of integrated circuits [12]. The proposed topology of a device allows tuning its conductivity type using a bias on the back gate and thereby optimizing the operation of a biosensor for recognizing different targets. The signals of analyte biomolecules of different types can differ depending on the size, charge, molecules location, distance, and the ionic strength and pH of the surrounding electrolyte solution [11,13,14]. An analytical model is presented that demonstrates the possibilities of using reconfigurable FET devices to recognize not only charged molecules, but also neutral ones [15].

Silicon attracts researchers, among other things, by the ease of its surface functionalization with chemical linkers [16,17], which makes it possible to use Si FETs for registering chemical events that occur on the NW surface. Owing to the high surface area-to-volume ratio, Si-NW FETs can efficiently convert signals and exhibit a high sensitivity. The receptor layer covering the surface of a transducer ensures specific binding of biomolecules from the test solution [4–7, 11, 16]. The receptor-functionalized Si-NW surface allows the reaction with an analyte in the test solution and the change in the surface charge resulting from the receptor–analyte interaction on the Si-NW surface can act as a monitored signal. The potentiometric sensing techniques for the sensitive detection of various molecules included in nucleic acids, proteins, macromolecules, bacteria, viruses, and living cells were reported [11,18]. The demonstrated label-free detection of low concentrations of biomarkers with Si-NW sensors attracts close attention due to the potential use in disease diagnosis and monitoring.

The efficiency of a biosensor as an analyte detector depends on the ability of the receptor–analyte pairs to change the surface charge density on the transducer layer. The biorecognition layer should be as thin as possible in order to localize the receptor–analyte binding events in the immediate vicinity of the gate oxide surface or, at best, within the Debye length  $\lambda_D$  [19]. Smaller receptor molecules (aptamers) are perfect for sensing the surface charge changes [13].

Aptamers are short (no more than 80 bases) single-chain ribo- or deoxyribo-oligonucleotides have a unique 3D structure formed by local complementary hairpins and the ionic, hydrophobic, and stacking interactions, which that provide binding affinity for molecular targets. Among the unquestionable advantages of aptamers are the simplicity of their modification in the course of chemical synthesis, a variety of targets (from ions to cellular compartments and whole cells), small size, high stability and, in some cases, specificity. All these properties make aptamer molecules highly preferable over antibodies in detection and binding to targets [20]. Aptamers, due to their small size, can hold targets close to Si-NWs and overcome the Debye length limitations for sensing small molecules and the high stability of aptamers in the environment makes them excellent candidates for use as receptor layers of solid-state biosensors. Moreover, due to the nucleotide structure of aptamers and molecule folding upon binding to targets, they enable the development of various aptasensors with improved analytical characteristics. By varying the type of an aptamer used, biosensors can be adjusted for targets of different types [21].

Universal platforms based on Si-NW FETs can be utilized to develop biosensors with high sensitivity [7]. Nevertheless, detection techniques employing Si-NW biosensors differ for nucleic acids, proteins, and microorganisms. A study by [22] used a thrombin-specific aptamer to specifically target thrombin and demonstrates the electrical detection of thrombin, a model biomarker, using arrays of Si-NWs. Aptasensors manufactured using the traditional top-down CMOS process can be used in various biomedical and biosensor applications. Development is underway to optimize sensor design to increase sensitivity and specificity. Simulation results [23] show that gate all around (GAA) Si-NW FETs are

superior to back-gated Si-NW FETs in terms of sensitivity for detecting DNA nucleotides. In another theoretical study [24] a complex design of GAA FET gates is considered, which requires laying gate oxides in two or more layers. The gate dielectric material plays a role in the design of the sensor during the formation of the receptor layer, and it affects the biosensor characteristics of FETs, as shown by calculations [25]. Theoretically, transistor designs have been analyzed that utilize high-k dielectric materials as the gate oxide and alternative materials such as GaAs, InGaAs and Ge for the channel, replacing silicon [26,27]. These designs incorporate the use of a nanogap cavity and present a challenge in filling this space with selective targeting for the desired biomolecules [3,10]. However, the proposed designs and calculations of their performance under various conditions provide hope for improving biosensors based on FET technology in the future.

The hFABP protein can serve as a biomarker for the early diagnosis of acute myocardial infarction [28]. The earliest detection of low concentrations of the acute myocardial infarction markers is extremely important, regardless of the patient gender and age, for the timely provision of necessary care. Several different immunosensors for the detection of hFABP have been described in the literature, which are based on antigen–antibody specific binding in combination with electrochemical or optical detection [29 – 31]. For the best our knowledge there are no reports about aptamer-based hFABP biosensors in the literature. In this work, a new DNA aptamer FABPp1c-t38, with high affinity to human hFABP [32], was used to functionalize Si-NWs.

In this study, we present for the first time the DNA aptamer-functionalized Si-NW CMOS transistors for detecting the heart-type fatty acid-binding protein (hFABP). The device was manufactured using the CMOS-compatible top-down technology, which involves the formation of NWs by lithography and reactive ion etching. The development of accessible diagnostic tools will ensure the progress in the creation of portable devices for early disease diagnosis.

## 2. Materials and methods

### 2.1. Materials

Sigma-Aldrich (3-Aminopropyl)triethoxysilane (APTES), dimethyl sulfoxide dihydrochloride (DMS), and Bicine ( $C_6H_{13}NO_4$ ) were used (<https://www.sigmaaldrich.com>). The 50 % APTES aqueous solution, 5 mg/mL DMS in 0.1 M Bicine (pH 8.5), and binding buffer (0.15 M NaCl,  $5 \times 10^{-2}$  M K-Na phosphate buffer pH 7.0 (PBS),  $1 \times 10^{-3}$  M  $MgCl_2$ ) were prepared. The amino derivative of the FABPp1c-t38 DNA aptamer ( $NH_2$ -5'-GACAAGACATCGGGAGGGAGGGAGGGCAGTCTAG TCT-3') was synthesized at the Laboratory of Synthetic Biology of the Institute of Chemical Biology and Fundamental Medicine, Siberian Branch of the Russian Academy of Sciences (Novosibirsk, Russia). Before use, the aptamer was refolded by heating to 90 °C for 5 min in the binding buffer with the subsequent cooling down to room temperature for 15 min. The recombinant hFABP was expressed and purified as described in [33].

### 2.2. Fabrication of the device

A multi-stage process of creating a Schottky barrier NW transistor using the top-down approach was described in detail in [34]. FET devices were fabricated using commercial boron-doped p-type silicon on insulator (SIMOX SOI) wafers with a resistivity of 18  $\Omega \cdot cm$  and a low doping level ( $10^{15} cm^{-3}$ ). The original 6-in. silicon-on-insulator (SOI) wafer was cut into 1-in. pieces. All subsequent technological operations were then carried out on these substrates. The silicon device layer thickness was 100 nm (the (100) orientation) and the buried oxide (BOX) layer thickness was 200 nm. The top silicon device layer was cleaned from native oxide and a 15 nm-thick Fe layer was deposited onto it (Fig. 1(a)) by thermal evaporation under ultrahigh vacuum conditions ( $10^{-8}$  Pa). The geometry of the devices was formed at the electron

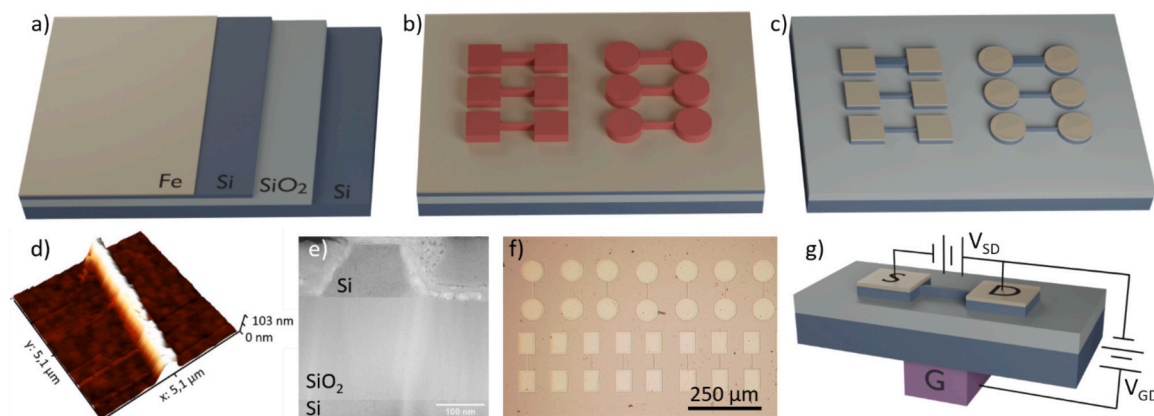


**Fig. 1.** Fabrication of the Si-NW transistor. (a) Deposition of the Fe film onto a SOI substrate, (b) formation of a mask by electron beam lithography, and (c) chemical etching of the Fe and Si layers followed by removal of the mask. (d) 3D AFM image and (e) TEM cross section of Si-NW with the indicated layers of materials. (f) Photograph of the device array. (g) Electrical property measurement scheme.

lithography stage (Fig. 1(b)); the parts of the Fe and Si layers not coated with the photoresist were removed by chemical etching (Fig. 1(c)). The widths of Si channels in the devices were  $W = 0.4, 1, \text{ and } 3 \mu\text{m}$  and the length of all the fabricated devices was  $L = 48 \mu\text{m}$ . The device parameters are shown in Table 1. Previously, the devices were tested and examined as protein biosensors in [35]. The same sensors were successfully reused. Before reusing the Si-NW FET chips, contaminants were removed from the surface by RCA chemical cleaning [36] in the  $\text{H}_2\text{O}:\text{H}_2\text{O}_2:\text{NH}_4\text{OH}$  solution (1,1,5, volume fractions) at a temperature of  $70^\circ$  for 10 min. When exposed to RCA, the organic compounds decomposed into volatile substances and water.

### 2.3. Si-NW surface functionalization

The covalent attachment of the recognition molecules (aptamers) was implemented through aminosilanization of native oxide on the Si-NWs surface [17] followed by using a homobifunctional dimethyl suberimidate (DMS) cross-linker. The complete chemical process of the surface functionalization in the Si-NW devices is outlined in Table 2. At *first stage*, a wafer with the devices was locally treated with the 50 % aqueous (4.27 M) APTES solution in the Si-NW region. To perform the local silanization of the surface, a CSG 01 AFM tip (<https://tipsnano.ru/>) was immersed in the APTES solution for 5 s and then blown with dry nitrogen to remove the excess solution. The silanization of Si NWs was performed using the dip-pen nanolithography techniques [37], which allows deposition of molecular layers onto appropriate substrates by transferring molecules from an AFM tip to a substrate via diffusion of molecules through the water meniscus connecting a tip and a substrate. The entire surface of the Si-NW was coated with APTES. For Si-NWs with  $W = 0.4, 1, \text{ and } 3 \mu\text{m}$ , the coating area was  $0.4 \times 48 \mu\text{m}^2, 1 \times 48 \mu\text{m}^2, \text{ and } 3 \times 48 \mu\text{m}^2$ . After the APTES deposition, the chips were incubated for 20 min and then the substrate with the chips was thoroughly washed with a 0.1 M Bicine solution (pH 8.5). The subsequent stages of the Si-NW surface modification were performed with a micropipette. DMS

**Table 1**

Design parameters of the device and their values.

Parameters	Value
Channel material	single crystal p-Si (100)
Doping concentration	$10^{15} \text{ cm}^{-3}$
Channel length (L)	$48 \mu\text{m}$
Channel widths (W)	0.4, 1, 3 $\mu\text{m}$
Body (Channel) thickness	100 nm
Gate oxide material	$\text{SiO}_2$
Recognition element	FABPAP1c-t38 aptamer
Analyte	hFABP

**Table 2**

Stages of the Si-NW surface modification.

Stage	Molecule	Coating	Incubation	Buffer
1	APTES	AFM tip	20 min. $T = 23 \pm 1^\circ\text{C}$ $H = 57 \pm 5\%$	0.1 M Bicine pH 8,5
2	DMS			
3	FABPAP1c-t38	pipette (2 $\mu\text{L}$ )		binding buffer
4	hFABP X pM			

X = 0, 1, 10, 100, 1000.

0 - binding buffer.

cross-linker, FABPAP1c-t38 aptamer receptor and the hFABP target analyte were attached in turn. At the *second stage*, 2  $\mu\text{L}$  of DMS was applied to the substrate using a mechanical micropipette and incubated for 20 min under controlled conditions of  $57 \pm 5\%$  humidity and  $23 \pm 1^\circ\text{C}$ . After that, the substrate was washed with binding buffer. At the *third stage*, receptor binding was performed, a 2  $\mu\text{L}$  drop of the FABPAP1c-t38 aptamer was applied using a micropipette, after that incubation was carried out for 20 min under the same conditions. Then, the substrate was washed again with a binding buffer. At the *fourth stage*, a 2  $\mu\text{L}$  droplet containing hFABP at various concentrations ( $X = 0, 1, 10, 100, \text{ and } 1000 \text{ pM}$ ) was applied to the substrate. The  $X = 0$  (binding buffer) was used as a control. Each time after application, a droplet containing target proteins was incubated for 20 min and then the substrate with the devices was thoroughly washed with a binding buffer. The sequence of the modification stages is given in Table 2. Additional AFM images are shown in Fig. S1 in the Supporting Information.

### 2.4. Electrical measurements

The electrical characteristics of the Si-NW devices were measured at a Lakeshore EMPX-HF 2 probe station under normal conditions ( $T = 297 \pm 3 \text{ K}$ ,  $H = 38 \pm 3\%$ ) using a Keithley 2634b SourceMeter two-channel instrument. The transfer characteristics were measured on three devices from four different arrays located on the same SOI wafer and fabricated in a single technological cycle. Using the data obtained, averaged values were calculated and the error (confidence intervals) at different transistor current channel widths (0.4, 1, and 3  $\mu\text{m}$ ) was determined.

The transistor was controlled by applying a voltage to the gate located on the backside of the substrate (back gate) and connected to it with an indium ohmic contact. The transistor is formed from the top silicon layer of the device and works as a converter, i.e., transmits the current through a channel between the Schottky source and drain Fe contacts. In this design of the device, the Si channel is left open, which allows using the transistor as a sensor. The Si channel is coated with a thin native  $\text{SiO}_2$  oxide layer, which comes into contact with molecules

(receptors and analytes) and acts as an electrical transducer when recording the physicochemical processes of binding target molecules. A typical device structure and a microscopic image are presented in Fig. 1 (f) and (g), respectively.

### 3. Results

#### 3.1. Si-NW surface treatment

##### 3.1.1. Local APTES deposition

Immobilization of receptors over the entire chip can result in binding of an analyte in large amounts to the surrounding Si-NW surface, rather than to the sensing element, which can reduce the sensitivity of a device [13]. Silicon oxidizes in air and, chemically, the nanowire surface is no different from the oxide on which Si-NWs were formed. At the conventional surface modification, APTES molecules (and, subsequently, the receptor) are immobilized over the entire surface. The presence of receptor molecules on the surface surrounding Si-NWs can lead to an indirect decrease in the nanowire biosensor sensitivity due to the fact that analyte molecules will bind to receptors outside the sensitive element. Since the amount of analyte hitting the sensitive element (Si-NW) will decrease, the concentration of the target molecule sample will have to be increased. Thus, the method for modifying the Si-NW FET surface seriously affects the sensitivity of detection of target molecules. APTES molecules bind to the hydroxyl-terminated SiO<sub>2</sub> NW surfaces with the formation of an amine-functionalized surface. To avoid immobilization of receptors over the entire chip surface, the Si-NW FET surface was locally modified with APTES molecules [38] using a tip of a

DPN 5000 NanoInk atomic force microscope in the contact scanning mode at a speed of  $\sim 2 \mu\text{m/s}$ . A method for the local surface modification using an AFM tip and an experiment with a biotin-streptavidin model system were reported previously in [35]. This approach can be used to implement biosensor devices consisting of an array of individually addressable Si-NWs with the functionalization of different types for simultaneous recognition of various targets.

To ensure continuous coverage of the Si-NW surface with APTES molecules, different speeds of the tip were tested and, then, the resulting areas were scanned in the lateral force microscopy (LFM) mode. The formation of a molecular layer can be visualized on a fluorescent microscope, but this would require additional fluorescent labeling of APTES with an amino modified fluorescent DNA [39]. In our case, the APTES deposition was monitored on the same device in the LFM mode, but at a higher tip speed, which is more convenient due to the precise positioning and ability to observe a molecular layer on a small surface area.

Fig. 2(a) schematically shows the APTES deposition areas in the contact mode (green frame) and scanning in the LFM mode (red frame). The topology image shows a part of the current channel of the transistor and the area covered with APTES. The tip speeds in different parts were  $V_{\text{tip1}} = 4 \mu\text{m/s}$ ,  $V_{\text{tip2}} = 2 \mu\text{m/s}$ , and  $V_{\text{tip3}} = 3 \mu\text{m/s}$ . The temperature ( $T$ ) and humidity ( $H$ ) were kept at  $23 \pm 1 \text{ }^\circ\text{C}$  and  $57 \pm 5 \%$ , respectively. AFM images of the topology of the Si-NW surface area and the corresponding LFM images obtained when moving the tip in the forward (Fig. 2(b)) and reverse (Fig. 2(c)) scanning passes show the presence of a molecular layer. According to the AFM data (Table s1 from SI), when processing substrate in 1 mL of the 50 % APTES aqueous solution at  $T =$

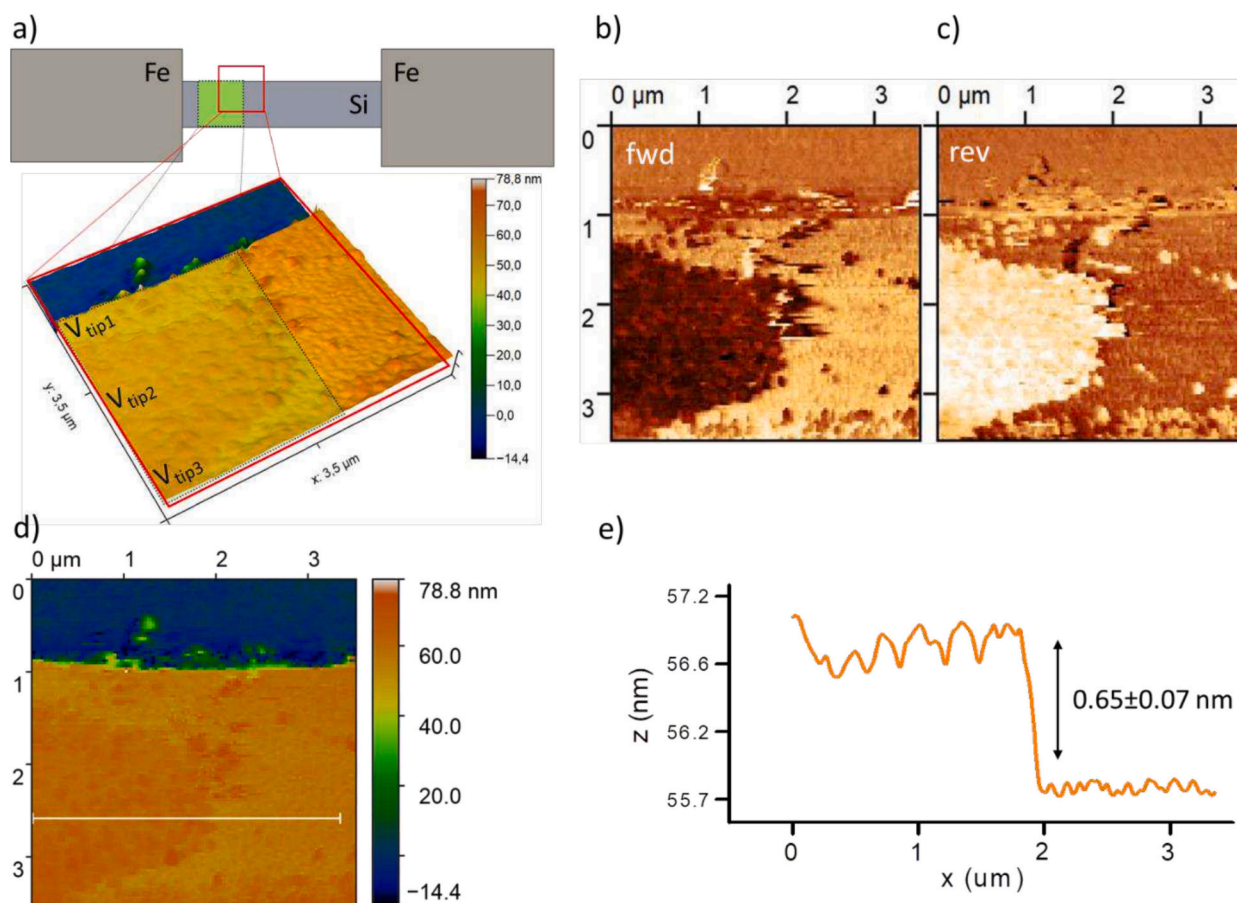


**Fig. 2.** (a) 3D AFM image of the topology with the schematically shown area of the APTES deposition at tip speeds of  $V_{\text{tip1}} = 4 \mu\text{m/s}$ ,  $V_{\text{tip2}} = 2 \mu\text{m/s}$ , and  $V_{\text{tip3}} = 3 \mu\text{m/s}$  (green frame). The green frame in the diagram indicates the scanning area after deposition of molecules. LFM images obtained with the tip moving in (b) the forward and (c) reverse scanning directions. (d) 2D AFM topology image and (e) cross-sectional profile of the surface obtained with the tip moving in (b) the forward and (c) reverse scanning directions. (For interpretation of the references to colour in this figure legend, the reader is referred to the web version of this article.)

22.6 °C for 40 min, APTES covers approximately 86.77 % of the Si surface. It should be noted that the functionalization process used to determine this value is somewhat different. In this case, a mechanical pipette was used to apply the APTES droplet, instead of the AFM tip. However, based on AFM and LFM images (Fig. 2), we assume that at least ~85 % of the entire Si-NWs surface is coated with APTES.

Importantly, while target capture probability from solution is proportional to surface area, only a small functionalized segment of the Si-NWs is required to induce the field effect. We propose that even a  $1 \times 1 \mu\text{m}^2$  APTES-coated area would be sufficient to activate the virtual (floating) gate effect in Si-NW CMOS devices, which in our system is mediated by the recognition molecule-target complex. Thus, the reported “~85 %” value specifically refers to the coating efficiency within this critical region. Due to steric effects, the relative surface coverage decreases for the aptamer (60.51 %) and hFABP (48.73 %). Nevertheless, we maintain that APTES plays the dominant role in device functionality, as the surface charge generating the virtual gate’s electric field is primarily established within this layer.

At the beginning and end of the deposition area (dotted lines), the tip speed was higher and, in the LFM images, one can see the areas that are free of molecules. When the tip moved at a higher speed, the rate of diffusion of molecules was insufficient to form a continuous layer. Fig. 2 (e) shows a profile, the height of which is in good agreement with the APTES molecule length ( $0.65 \pm 0.07$  nm). This suggests that the monomolecular APTES layer can be obtained, which is of crucial importance for the successful covalent binding of subsequent molecules. The formation of the monomolecular APTES layer is necessary for controlling immobilization of receptors and avoiding binding of a large amount of the analyte on the surrounding Si-NW surface, rather than on the transistor channel, which can reduce the sensitivity of the device.

To manipulate small amounts of the reagents, microfluidic devices

are widely used, which usually consist of channels with a width ranging from tens to hundreds of micrometers [40]. The small size of Si NWs allows the integration of multiple sensors into a microfluidic channel. On the other hand, when FETs are reduced to the nanosize, combining a chip with a microfluidic system becomes a technological challenge and enhances the production cost. Without complex microfluidic systems, sensors could be easier and more cost-effective to produce in large quantities, and they could also be more durable and reusable. In this work, 2- $\mu\text{L}$  droplets of the solutions containing the required molecules were used. The drop in drop assay simplifies the manufacture and makes it possible to use ultra-small sample volumes. This approach can be used to develop the techniques of detection using FETs sensors under dry conditions, which is promising owing to the simple scheme for applying receptor labels and the need for a small amount of analyte. From a practical standpoint, this can help in the creation of wearable electronics and compact LoC systems.

### 3.2. Electrical detection

#### 3.2.1. Response of the devices upon binding a chain of molecules

The electrical measurements were carried during functionalization and after addition of targets using a scheme presented in Fig. 1(g). At each modification stage, the  $I$ - $V$  characteristics were measured, which had a shape typical of devices of this kind, demonstrating the ambipolar transistor open state with increasing gate voltage, regardless of the voltage sign (Fig. 3(a)). The similar behavior of all the transfer characteristics allowed us to state the successful binding of molecules and to monitor the efficiency of each functionalization stage. Fig. 3(a) shows the transfer characteristics of the devices with a current channel width of  $0.4 \mu\text{m}$ . The source-drain current  $I_{SD}$  was measured as a function of the gate voltage  $V_G$  in the range from  $-14$  V to  $14$  V at a fixed

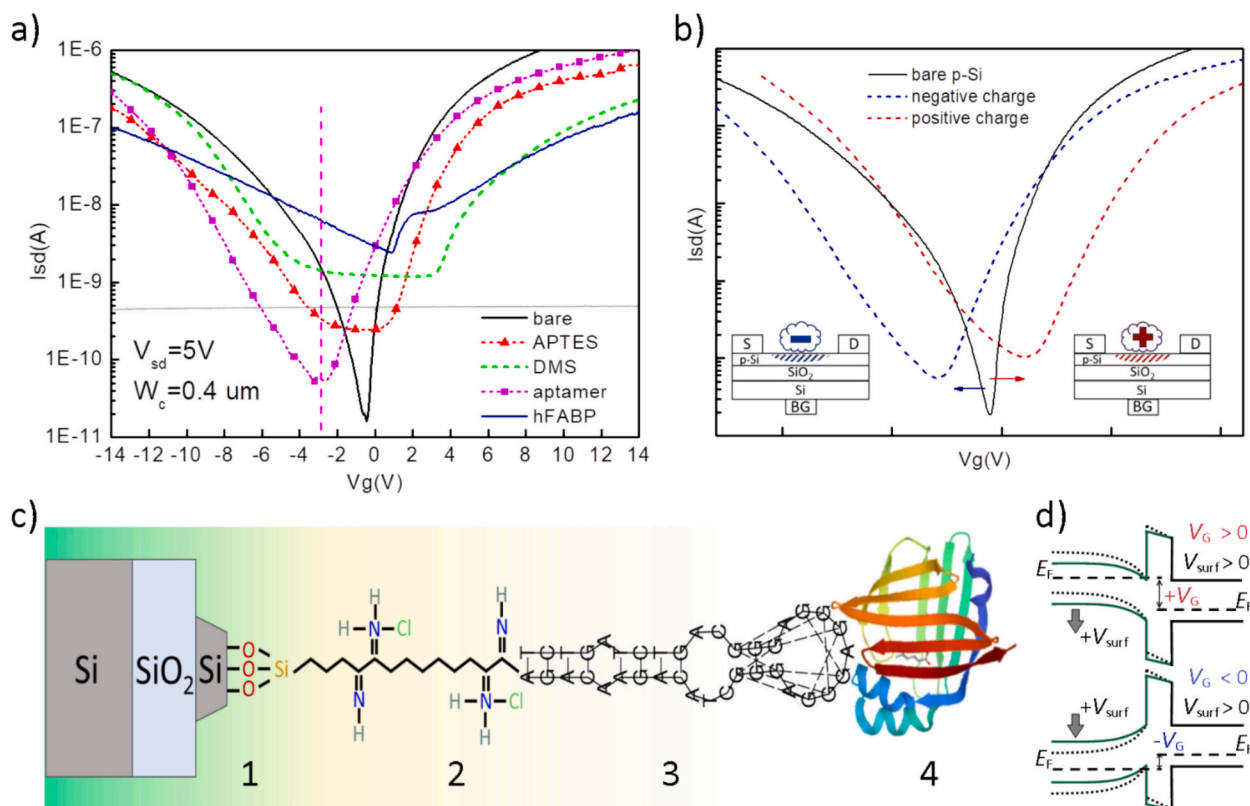


**Fig. 3.** (a) Transfer characteristics of Si NWs at each stage of the surface functionalization of the transistor current channel. The gate current level is marked in gray. (b) Diagram of the effect of the molecular charge on the offset of the transfer characteristic of the transistor. (c) Schematic of the chemical functionalization of the Si-NW surface. Numbers correspond to the modification stages in Table 2: (1) APTES, (2) DMS, (3) aptamer, and (4) hFABP. (d) Band diagrams of inversion (top) and accumulation (bottom) modes of FETs.

source–drain bias of  $V_{SD} = 5$  V. The solid and dotted lines show the source current  $I_{SD}$  as a function of the applied gate voltage  $V_G$  on the logarithmic scale (along the  $x$  axis) for the clean (bare) device and for each stage of addition of molecules. First, after the cleaning stage, the signal of the bare devices without APTES functionalization was detected. Second, after the APTES deposition, incubation, and removal of excess molecules, the second signal was measured. In the case of the clean device, a slight voltage shift corresponding to the minimum  $I_{SD}$  current, i.e., the transistor off-state (at the threshold voltage  $V_{th}$ ), towards negative values is observed during the surface silanization. At the third stage, the cross-linker was added and the DMS signal was measured. The addition of DMS leads to a shift of the transfer characteristic towards positive values relative to the previous stage. The fourth stage is a signal after attachment of recognition receptor (aptamer) molecules. The presence of the FABP<sub>ap1c-t38</sub> aptamer leads to a significant shift of the signal towards negative values and, in addition, the shape of the curve slightly changes. At the fifth stage, 2  $\mu$ L of the hFABP sample in the binding buffer (1000 pM) was added to the devices and its effect on the behavior of the transfer characteristics of the devices was monitored.

The behavior of the  $I$ – $V$  characteristic is the same for all the investigated devices and is qualitatively independent of the FET channel width. Due to the specificity of the experimental design, the  $V_{th}$  shift in the Si-NW transfer characteristics was monitored as a detection signal. The measurements of the transfer characteristics of the adjacent structures showed that, without the APTES modification, binding does not occur and the characteristics correspond to the bare signal of the unmodified devices. For this purpose, reference devices were used (Fig. 1 (f), circular contact pads) located nearby and formed under the same conditions, but not treated with APTES using the AFM tip (Fig. S2 in Supporting Information).

Binding of the functionalizing or detectable molecules on the surface of the Si-NW device changes the effective surface charge at the silicon–air interface, which, in turn, affects the threshold and on-current of a FET. If a detected molecule is positively charged, it creates a space charge cloud around itself, which acts like a floating gate [41] and leads to a change in the threshold voltage of the transistor and a shift of its transfer characteristic to the positive region, and vice versa (Fig. 3(b)). Without a microfluidic system, the current in the channel of the device can be affected by different factors, including the humidity, ambient temperature, and contamination. However, we should detect the corresponding molecules in the space surrounding the current channel by changing  $V_{th}$ . Specific changes in  $V_{th}$  are related to the changes in the total polarization of the molecular chain shown in Fig. 3(c) or, in other words, with the value and sign of the surface potential at the APTES/native oxide interface. The case of negatively charged molecules was described for these devices in more detail in [35]. When target molecules are charged positively, the nanowire surface acquires a positive charge. This additional charge modulates bending of the energy bands, slightly shifting them downward. This leads to an increase in the current in the transistor inversion mode, since the conduction bands at the interface move closer to the Fermi level, which leads to an increase in the concentration of the two-dimensional electron gas (upper diagram in Fig. 3(d)). In contrast, in the accumulation mode, the hole current weakens, since the valence band edge approaches the Fermi level of holes, which leads to a decrease in the two-dimensional hole gas concentration (lower diagram in Fig. 3(d)). The combined effect of these two mechanisms is manifested in a characteristic shift of the transfer characteristics (Fig. 3(d), transfer characteristic with a shift from “+” and “–” molecules).

### 3.2.2. hFABP detection

The number of charged molecules and the fact of their binding to the oxide surface of the transistor channel can be directly detected as a change in the subthreshold slope or a shift in the threshold voltage  $V_{th}$  or the  $I_{sd}$  change. In different works, authors used different approaches; for example, the  $I_{sd}$  value can be affected by many factors, e.g., humidity

[42], solution pH, and others [13,43,44], especially when measured under dry conditions. Therefore, in all the detection experiments, we ignored the resistance/current value and focused only on the change in  $V_{th}$ , which will be largely affected by the change in the effective potential on the surface of the transistor current channel. This approach allowed us to obtain the concentration dependences of the  $V_g$  shift. When measuring this shift relative to the previous concentration, we obtain a detector sensitive to the presence of target molecules. Fig. 4(a) shows the transfer characteristics of the devices after incubation with the hFABP target protein in different concentrations (1–1000 pM) at a transistor current channel width of 0.4  $\mu$ m. Depending on the protein concentration, a fixed shift of the  $I_{sd}$  minimum position is observed.

For the devices with wider current channels, the pronounced minimum is not always observed and the bottom of the transfer characteristic is an extended flat region, as can be seen for the APTES and DMS signal in Fig. 3(a). In this case, to determine the  $V_{th}$  position, a difference between the  $V_G$  values in the left- and right-hand curves at the fixed  $I_{sd}$  value was taken, which exceeded the minimum current by 15 %. When monitoring the change in the  $V_{th}$  value at different concentrations, we observe a shift with the addition of the next probe at a certain concentration (Fig. 4(a)). By plotting the  $V_{th}$  shift versus  $V_{th}$  at different hFABP concentrations, one can easily obtain the concentration dependence of the sensor sensitivity (Fig. 4(b)). It should be noted that the  $V_{th}$  shift was plotted after a series of experiments, including those with a different device array and taking into account the errors. Aptamer we used has high specificity to hFABP: as shown in [32] it does not bind to major serum proteins such as human serum albumin and immunoglobulins, as well as to whole human serum, so it can be applied as recognition molecule for hFABP detection and binding.

The buffer with the zero-target concentration was measured first; it can be seen that ions in the PBS solution weakly affect the change in the  $V_{th}$  value, which is indicative of the correct choice of the monitored parameter. When a solution with a target concentration of 1 pM is added, a change in the  $V_{th}$  value is observed. At 0.4 and 1  $\mu$ m, the shift is obvious and easy to measure, but, for a wider channel (3  $\mu$ m), the change is negligible and the measured value lies within a wide confidence interval. As the target concentration grows to 10 pM and above, all the devices exhibit a good response and an increase in the  $V_{th}$  shift with concentration. The next experiment showed that, at a concentration of 3125 pM, the sensor stops responding, which can be interpreted as saturation. This experiment clearly shows that the proposed chain of APTES–DMS aptamer molecules can bind the hFABP and hold them close to the Si-NW surface, providing an electric field sufficient to change the measured electrical parameters of the Si-NW device.

In the label-free detection of analytes based on charge detecting, the sensitivity of a sensor measured in liquid media depends on the ionic strength of a buffer. In dilute buffers, when the charge screening effect is minimized and the  $\lambda_D$  value exceeds 10 nm, the  $V_{th}$  shift increases significantly. Choi et al. studied the effect of the environment on the detection of charged molecules using Si-NW FETs [42]. At the measurements in the dry environment, the sensitivity is higher, but there can be some instability during the measurements. In this work, this effect was avoided by incubating molecules in a liquid droplet for the time sufficient for the uniform distribution.

The average sensitivity of the sensors can be determined from the slope of the linear regions in Fig. 4(d) as a change in the signal  $\Delta V_g$  divided by the target concentration increment [45]. It can be seen that the devices with a 0.4  $\mu$ m-wide current channel are the most sensitive; a lower target concentration results in a stronger  $V_{th}$  change. The average sensitivity of the sensor calculated from the slope of the plot was found to be  $\sim 0.33$  V/pM. The  $V_{th}$  shift is more sensitive at low concentrations and therefore the devices with a 0.4  $\mu$ m-wide current channel are more efficient in detecting low concentrations of targets. At the same time, the devices with a 0.4  $\mu$ m-wide current channel are noticeably susceptible to environmental factors, responding to the humidity and pressure specified in the experiment (Fig. 4(a), 1 pM concentrations). Devices with 1-

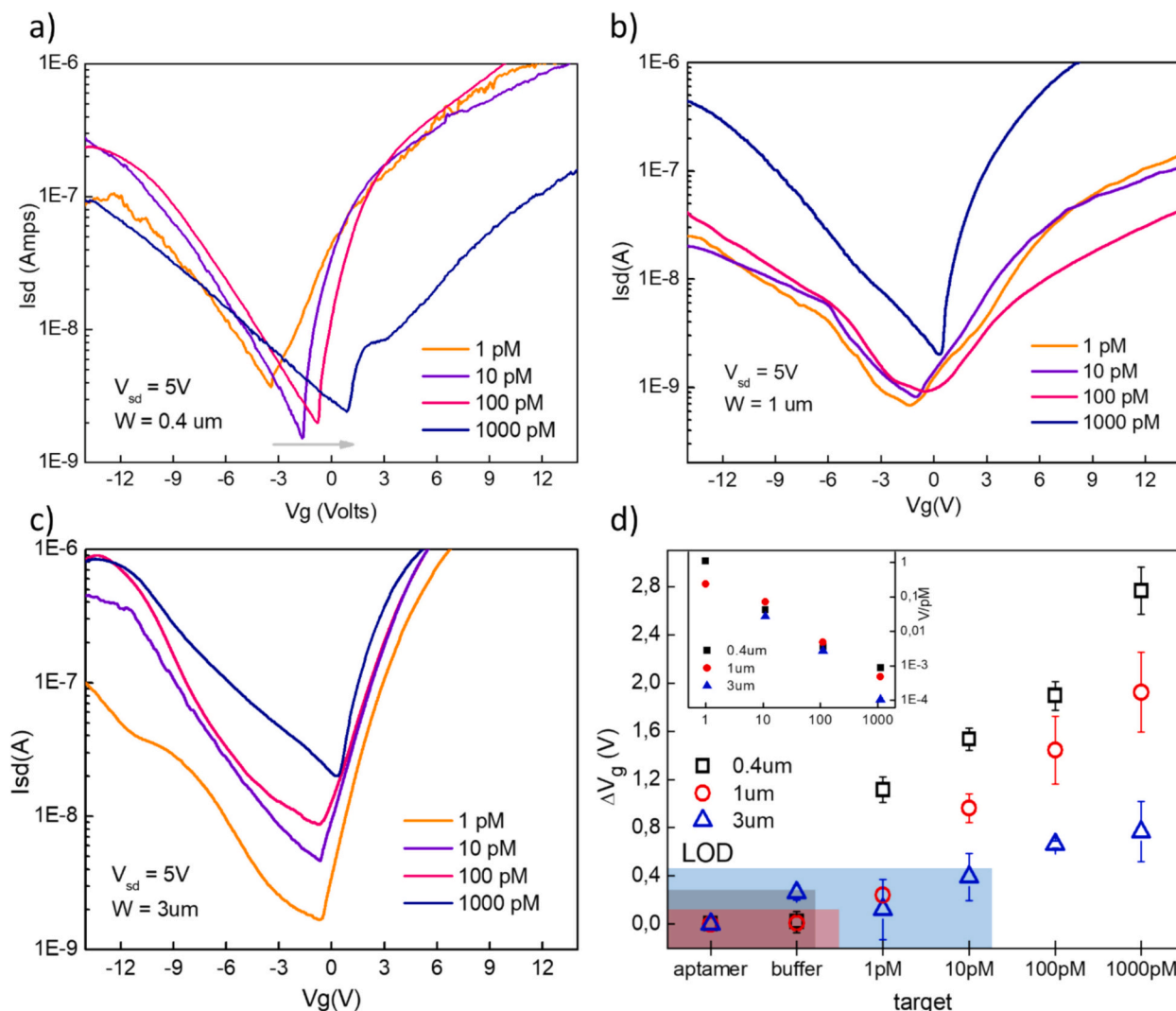


**Fig. 4.** Transfer characteristics of the Si-NW FET in the amplification mode at different concentrations (from 1 pM to 1000 pM) of target molecules for (a) 0.4  $\mu\text{m}$ ; (b) 1  $\mu\text{m}$  and (c) 3  $\mu\text{m}$ , respectively. (d) Plot of the  $V_g$  shift for different concentrations of target molecules. The LOD is marked in the plot in different colors: 0.04, 0.54, and 21.38 pM for the devices with a channel width of 0.4, 1, and 3  $\mu\text{m}$ , respectively. The inset shows the sensitivity (V/pM) plot for different devices in different concentration ranges.

and 3- $\mu\text{m}$  channels can be easily fabricated using traditional optical lithography and can still provide sufficient sensitivity for measurements under dry conditions. Devices with a 1- $\mu\text{m}$  current channel exhibit a sufficient sensitivity ( $\sim 0.18$  V/pM), especially in the concentration range of 1–100 pM, and can be easily manufactured using conventional lithographic techniques. The devices with a current channel width of 3  $\mu\text{m}$  exhibit, as expected, the lowest sensitivity ( $\sim 0.07$  V/pM), but can be used in long-term measurements, when it is necessary to detect a great number of targets, for example, in a continuous flow. The limit of detection (LOD) for the devices of each type is marked in Fig. 4(d) with a colored rectangle. The LOD is generally estimated using the 3-sigma method [46,47] where the LOD is defined as the hFABP concentration that corresponds to the sensor response equal to three standard deviations of the blank sample (i.e., the binding buffer only).

Since the durability of the devices depends on the current channel width, when manufacturing commercial reusable devices, it is important to strike a balance between the energy efficiency, sensitivity, and reusability. Kudo et al. examined the durability characteristics of devices and showed that the number of operating cycles before destruction of the oxide increases with decreasing channel width [48]. However, speaking about the use of transistors as biosensors and operation in a biological environment, the use of thin NWs can lead to their thinning and even

destruction. As shown in [49], the improved long-term stability can be obtained by coating NWs with  $\text{Al}_2\text{O}_3$ . However, the protective coating reduces the sensitivity of Si NWs and, among other things,  $\text{Al}_2\text{O}_3$  degrades in liquid media. The use of wide transistor channels facilitates the durability of the devices. For the biosensing applications, NRs are preferred for quantifying analyte concentrations, because the probability of the analyte binding increases linearly with the available surface area. The devices, functionalization, and detection scheme presented by us have several advantages over the previously proposed methods for using Si NWs.

#### 4. Conclusions

A set of FETs with Si-NW widths of 0.4, 1, and 3  $\mu\text{m}$  and a length of 48  $\mu\text{m}$  were fabricated. The local functionalization of Si-NWs by the receptors consisting of a system of three molecules (APTES, DMS, and aptamer) was performed. In this study, we demonstrated a potential approach for biomolecule immobilization on the current channel of a Si-NW FET using an AFM tip. The local APTES modification was carried out using an AFM tip in the contact scanning mode at a speed of  $\sim 2$   $\mu\text{m}/\text{s}$ . The FABPAP1c-t38 aptamer, being specific for the target hFABP biomarker, ensures the binding, leading to a change in the electrical

potential on the Si-NW surface observed as a shift in the transfer characteristic of the transistor. After the hFABP incubation in a model buffer solution, the opening voltage  $V_{th}$  of the transistor shifts from 0.1 to 2.8 V, which makes it possible to use this signal to detect the hFABP in concentrations of 1 pM (14.5 pg/mL). The fabricated Si-NW FET sensors did not show noticeable electrical or chemical aging during the operation, measurements, functionalization, and cleaning (Fig. S3, in Supporting Information). The highest sensitivity was established for the devices with a transistor channel width of 0.4  $\mu\text{m}$ . However, the Si-NW FETs with a channel width of 1  $\mu\text{m}$  and 3- $\mu\text{m}$  can be easily fabricated by conventional optical lithography and still able to detect the cardiac biomarker in a concentration of 1 pM. Thus, the fundamental feasibility detection of the hFABP target by the developed Si-NW FET aptasensor in the dry environment after incubation in the model buffer solution was demonstrated. Although the current in the channel of the device can be affected by various factors, including the humidity and ambient temperature, the presence of the corresponding molecules in the space surrounding the current channel was successfully detected by a change in the  $V_{th}$  value. The next step of our research will be to test the applicability of the developed sensor for detecting hFABP in complex biological samples, including clinical samples. To our knowledge it is the first aptamer-based electrosensor for hFABP detection. The selective electrical detection scheme based on the Si-NW FET and the aptamer can be extended to other targets, such as various cells, proteins, and low-molecular compounds, using aptamers with the appropriate specificity. This approach has the potential for application not only in medicine, but also in other fields: food industry, agriculture, ecology, etc. The results of the study of the behavior of the Si-NW FET sensors in the air environment can also be used to design various sensors integrated into wearable devices.

#### CRedit authorship contribution statement

**Anna Lukyanenko:** Writing – original draft, Investigation, Formal analysis. **Lev Shanidze:** Investigation. **Vasilisa Krasitskaya:** Writing – review & editing, Conceptualization. **Olga Vshivkova:** Investigation. **Ludmila Frank:** Writing – review & editing. **Anton Tarasov:** Writing – review & editing, Supervision.

#### Declaration of competing interest

The authors declare that they have no known competing financial interests or personal relationships that could have appeared to influence the work reported in this paper.

#### Acknowledgements

This study was carried out within the State Assignment of the Ministry of Science and Higher Education of the Russian Federation for the Krasnoyarsk Scientific Center, Siberian Branch of the Russian Academy of Sciences.

#### Appendix A. Supplementary data

Supplementary data to this article can be found online at <https://doi.org/10.1016/j.microc.2025.114358>.

#### Data availability

No data was used for the research described in the article.

#### References

- [1] P. Bergveld, Development of an ion-sensitive solid-state device for neurophysiological measurements, *IEEE Trans. Biomed. Eng. BME-17* (1970) 70–71, <https://doi.org/10.1109/TBME.1970.4502688>.
- [2] F. Andrieu, Planar fully depleted (FD) silicon-on-insulator (SOI) complementary metal oxide semiconductor (CMOS) technology, silicon-on-insulator (SOI), *Technology 5* (2014) 124–166, <https://doi.org/10.1533/9780857099259.1.124>.
- [3] A. Das, S. Rewari, B.K. Kanaujia, R.S. Gupta, Recent technological advancement in surrounding gate MOSFET for biosensing applications—a synoptic study, *Silicon 14* (10) (2022) 5133–5143, <https://doi.org/10.1007/s12633-021-01288-w>.
- [4] P.R. Nair, M.A. Alam, Design considerations of silicon nanowire biosensors, *IEEE Trans. Electron Devices 54* (2007) 3400–3408, <https://doi.org/10.1109/TEDE.2007.909059>.
- [5] J.M. Ziegler, I. Andoni, E.J. Choi, L. Fang, H. Flores-Zuleta, N.J. Humphrey, D. Kim, J. Shin, H. Youn, R.M. Penner, Sensors based upon nanowires, nanotubes, and nanoribbons: 2016–2020, *Anal. Chem. 93* (2020) 124–166, <https://doi.org/10.1021/acs.analchem.0c04476>.
- [6] A. Kumar, S. Kale, Spacer-engineered reconfigurable silicon nanowire schottky barrier transistor as a label-free biosensor, *Silicon 16* (5) (2024) 2023–2036, <https://doi.org/10.1007/s12633-023-02812-w>.
- [7] H. Li, D. Li, H. Chen, X. Yue, K. Fan, L. Dong, G. Wang, Application of silicon nanowire field effect transistor (SiNW-FET) biosensor with high sensitivity, *Sensors 23* (15) (2023) 6808, <https://doi.org/10.3390/s23156808>.
- [8] P. Goyal, G. Srivastava, J. Madan, R. Pandey, R.S. Gupta, Analytical modelling and reliability analysis of charge plasma-assisted Mg<sub>2</sub>Si/Si heterojunction doping less DGTFFET for low-power switching applications, *Phys. Scr. 99* (1) (2023) 015008, <https://doi.org/10.1088/1402-4896/ad1232>.
- [9] A. Bhardwaj, P. Kumar, B. Raj, N. Kumar, S. Anand, Design and optimization of vertical nanowire tunnel FET with electrostatic doping, *Eng. Res. Express 5* (4) (2023) 045025, <https://doi.org/10.1088/2631-8695/acff3a>.
- [10] A. Das, S. Rewari, B.K. Kanaujia, S.S. Deswal, R.S. Gupta, Analytical investigation of a triple surrounding gate germanium source metal–oxide–semiconductor field-effect transistor with step graded channel for biosensing applications, *international journal of numerical modelling: electronic networks, Dev. Fields 36* (6) (2023) e3106, <https://doi.org/10.1002/jnm.3106>.
- [11] M.O. Noor, U.J. Krull, Silicon nanowires as field-effect transducers for biosensor development: A review, *Anal. Chim. Acta 825* (2014) 1–25, <https://doi.org/10.1016/j.aca.2014.03.016>.
- [12] U. Schwalke, T. Krauss, F. Wessely, Dopant-free CMOS on SOI: multi-gate Si-nanowire transistors for logic and memory applications, *ECS Trans. 53* (2013) 105, <https://doi.org/10.1149/05305.0105ecst>.
- [13] D. Rani, V. Pachauri, S. Ingebrandt, Silicon nanowire field-effect biosensors, *Adv. Mater. Dev. Appl. 16* (2018) 27–57, [https://doi.org/10.1007/5346\\_2017\\_19](https://doi.org/10.1007/5346_2017_19).
- [14] B. Sharma, S. Yadav, S. Rewari, Y. Hasija, DM-PA-CNTFET biosensor for breast cancer detection: analytical model, *ECS J. Solid State Sci. Technol. 13* (8) (2024) 087004, <https://doi.org/10.1149/2162-8777/ad6a88>.
- [15] V. Thakur, A. Kumar, S. Kale, Analytical modeling of spacer-engineered reconfigurable silicon nanowire Schottky barrier transistor for biosensing applications //Micro and nanostructures, *Micro Nanostruct. 188* (2024) 207799, <https://doi.org/10.1016/j.micrna.2024.207799>.
- [16] Y. Cui, Q. Wei, H. Park, C.M. Lieber, Nanowire nanosensors for highly sensitive and selective detection of biological and chemical species, *Science 293* (2001) 1289–1292, <https://doi.org/10.1126/science.1062711>.
- [17] D. Kim, H. Lee, H. Jung, S. Kang, Single-protein molecular interactions on polymer-modified glass substrates for Nanoarray Chip application using dual-color TIRFM, *Bull. Korean Chem. Soc. 28* (2007) 783–790, <https://doi.org/10.5012/bkcs.2007.28.5.783>.
- [18] B. Li, C. Chen, U.R. Kumarac, Y. Chen, Advances in nanowire transistors for biological analysis and cellular investigation, *Analyst 139* (2014) 1589–1608, <https://doi.org/10.1039/C3AN01861J>.
- [19] G. Zhang, G. Zhang, J. Chua, R. Chee, E. Wong, A. Agarwal, K.D. Buddharaju, N. Singh, Z. Gao, N. Balasubramanian, DNA sensing by silicon nanowire: charge layer distance dependence, *Nano Lett. 8* (2008) 1066–1070, <https://doi.org/10.1021/nl072991l>.
- [20] H. Yoo, H. Jo, S. Oh, Detection and beyond: challenges and advances in aptamer-based biosensors, *materials, Advances 1* (2020) 2663–2687, <https://doi.org/10.1039/D0MA00639D>.
- [21] J. Lee, H. Jin, M.S. Desai, S. Ren, S. Kim, S. Lee, Biomimetic sensor design, *Nanoscale 7* (2015) 18379–18391, <https://doi.org/10.1039/C5NR05226B>.
- [22] R. Midahuen, V. Stambouli, C. Fontelaye, G. Nonglaton, N. Spinelli, S. Barraud, Aptasensors based on silicon nanowire field-effect transistors for electrical detection of thrombin, *Microelectron. Eng. 286* (2024) 112130, <https://doi.org/10.1016/j.mee.2023.112130>.
- [23] A. Wasfi, N. Alnaji, A. Mustafa, F. Awwad, Detection of DNA nucleotides via silicon nanowire field-effect transistor sensors with a nanogap: semi-empirical modeling, *AEU Int. J. Electron. Commun. 173* (2024) 154983, <https://doi.org/10.1016/j.aeu.2023.154983>.
- [24] A. Das, B.K. Kanaujia, V. Nath, S. Rewari, R.S. Gupta, Impact of reverse gate oxide stacking on gate all around tunnel FET for high frequency analog and RF applications, in: 2020 IEEE 17th India Council International Conference (INDICON), IEEE, 2020, pp. 1–6, <https://doi.org/10.1109/INDICON49873.2020.9342175>.
- [25] A. Das, S. Rewari, B.K. Kanaujia, S.S. Deswal, R.S. Gupta, Numerical modeling of a dielectric modulated surrounding-triple-gate germanium-source MOSFET (DM-STGGS-MOSFET)-based biosensor, *J. Comput. Electron. 22* (2) (2023) 742–759, <https://doi.org/10.1007/s10825-023-02008-w>.
- [26] V.K. Chappa, A.K. Yadav, A. Deka, R. Khosla, Investigating the effects of doping gradient, trap charges, and temperature on Ge vertical TFET for low power switching and analog applications, *Mater. Sci. Eng. B 299* (2024) 116996, <https://doi.org/10.1016/j.mseb.2023.116996>.

- [27] S. Yadav, S. Rewari, Dielectric modulated gallium-arsenide gate-all-around engineered field effect transistor (GaAs-GAAE-FET) biosensor for breast cancer, in: 2024 IEEE International Conference on Computing, Power and Communication Technologies (IC2PCT), IEEE, 2024, pp. 1553–1557, <https://doi.org/10.1109/IC2PCT60090.2024.10486515>. T. 5. – C.
- [28] M. Moon, C. Yoon, K. Lee, S. Kang, T. Youn, I. Chae, Evaluation of heart-type fatty Acidbinding protein in early diagnosis of acute myocardial infarction, *J. Korean Med. Sci.* 36 (2021) 1–12, <https://doi.org/10.3346/jkms.2021.36.e61>.
- [29] C.M. Prado, P.A. Burgos Ferreira, L. Alves de Lima, E.K. Gomes Trindade, R. Fireman Dutra, A methylene blue-enhanced nanostructured electrochemical Immunosensor for H-FABP myocardial injury biomarker, *Biosensors* 13 (9) (2023) 873, <https://doi.org/10.3390/bios13090873>.
- [30] N.A. Taranova, A.A. Bulanaya, A.V. Zherdev, B.B. Dzantiev, Triple enhancement for sensitive Immunochromatographic assay: A case study for human fatty acid-binding protein detection, *Biosensors* 12 (12) (2022) 1166, <https://doi.org/10.3390/bios12121166>.
- [31] Z. Shi, Z. Xu, J. Hu, W. Wei, X. Zeng, W.-W. Zhao, P. Lin, Ascorbic acid-mediated organic photoelectrochemical transistor sensing strategy for highly sensitive detection of heart-type fatty acid binding protein, *Biosens. Bioelectron.* 201 (2022) 113958, <https://doi.org/10.1016/j.bios.2021.113958>.
- [32] V.V. Krasitskaya, T.A. Vereshchagina, T.E. Smoliarova, A.E. Sokolov, A.E. Tupikin, Arca V. Dominguez, L.A., Frank development and characterization of novel DNA aptamers specific to heart-type fatty acid binding protein (hFABP), *J. Sib. Fed. Univ. Biol.* 17 (3) (2024) 302–319. <https://elib.sfu-kras.ru/handle/2311/153849>.
- [33] V.V. Krasitskaya, M.K. Efremov, L.A. Frank, Luciferase NLuc site-specific conjugation to generate reporters for in vitro assays, *Bioconjug. Chem.* 34 (2023) 1282–1289, <https://doi.org/10.1021/acs.bioconjchem.3c00165>.
- [34] A.V. Lukyanenko, A.S. Tarasov, L.V. Shanidze, M.N. Volochaev, F.V. Zelenov, I. A. Yakovlev, I.A. Bondarev, N.V. Volkov, Technique for fabricating ferromagnetic/silicon active devices and their transport properties, *Journal of surface investigation: X-ray, synchrotron and neutron, Techniques* 15 (2021) 65–69, <https://doi.org/10.1134/S1027451021010109>.
- [35] T.E. Smoliarova, L.V. Shanidze, A.V. Lukyanenko, F.A. Baron, V.V. Krasitskaya, A. S. Kichkailo, A.S. Tarasov, N.V. Volkov, Protein biosensor based on Schottky barrier nanowire field effect transistor, *Talanta* 239 (2022) 123092, <https://doi.org/10.1016/j.talanta.2021.123092>.
- [36] S. Wolf, R. Tauber, *Silicon Processing for the VLSI Era, Vol. 1: Process Technology*, Lattice Press, CA, 1986.
- [37] J. Haaheim, R. Eby, M. Nelson, J. Fragala, B. Rosner, H. Zhang, G. Athas, Dip pen nanolithography (DPN): process and instrument performance with Nanolink's Nscriptor system, *Ultramicroscopy* 103 (2005) 117–132, <https://doi.org/10.1016/j.ultramicro.2004.11.015>.
- [38] B. Li, C. Chen, W. Yang, T. Lin, C. Pan, Y. Chen, Biomolecular recognition with a sensitivity-enhanced nanowire transistor biosensor, *Biosens. Bioelectron.* 45 (2013) 252–259, <https://doi.org/10.1016/j.bios.2013.02.009>.
- [39] J. Schütt, B. Ibarlucea, R. Illing, F. Zörgiebel, S. Pregl, D. Nozaki, W.M. Weber, T. Mikolajick, L. Baraban, G. Cuniberti, Compact nanowire sensors probe microdroplets, *Nano Lett.* 16 (2016) 4991–5000, <https://doi.org/10.1021/acs.nanolett.6b01707>.
- [40] C. Kung, H. Gao, C. Lee, Y. Wang, W. Dong, C. Ko, G. Wang, L. Fu, Microfluidic synthesis control technology and its application in drug delivery, bioimaging, biosensing, environmental analysis and cell analysis, *Chem. Eng. J.* 399 (2020) 125748, <https://doi.org/10.1016/j.cej.2020.125748>.
- [41] O.V. Naumova, M.A. Il' nitskiĭ, L.N. Safronov, V.P. Popov, Silicon-on-insulator nanotransistors with two independent gates, *Semiconductors* 41 (2007) 103–109, <https://doi.org/10.1134/S1063782607010198>.
- [42] H. Choi, D. Shin, J. Lee, H. Mo, T. Park, B. Park, D. Kim, S. Choi, D. Kim, J. Park, The analysis of characteristics in dry and wet environments of silicon nanowire-biosensor, *J. Nanosci. Nanotechnol.* 16 (2016) 4901–4905, <https://doi.org/10.1166/jnn.2016.12247>.
- [43] R.B.M. Schasfoort, P. Bergveld, R.P.H. Kooyman, J. Greve, Possibilities and limitations of direct detection of protein charges by means of an immunological field-effect transistor, *Anal. Chim. Acta* 238 (1990) 323–329, [https://doi.org/10.1016/S0003-2670\(00\)80554-1](https://doi.org/10.1016/S0003-2670(00)80554-1).
- [44] M. Schöning, A. Poghosian (Eds.), *Label-Free Biosensing*. Springer Series on Chemical Sensors and Biosensors vol. 16, Springer, Cham, 2018, <https://doi.org/10.1007/978-3-319-75220-4>.
- [45] B.A. Prabowo, P.D. Cabral, P. Freitas, E. Fernandes, The challenges of developing biosensors for clinical assessment: A review, *Chemosensors* 9 (2021) 299, <https://doi.org/10.3390/chemosensors9110299>.
- [46] K. Pimková, M. Bocková, K. Hegnerová, J. Suttar, J. Čermák, J. Homola, J.E. Dyr, Surface Plasmon resonance biosensor for the detection of VEGFR-1—a protein marker of myelodysplastic syndromes, *Anal. Bioanal. Chem.* 402 (2012) 381–387, <https://doi.org/10.1007/s00216-011-5395-3>.
- [47] D. Kim, C. Park, W. Choi, S. Shin, B. Jin, R. Baek, J. Lee, Improved long-term responses of Au-decorated Si nanowire FET sensor for NH<sub>3</sub> detection, *IEEE Sensors J.* 20 (2019) 2270–2277, <https://doi.org/10.1109/JSEN.2019.2952582>.
- [48] T. Kudo, T. Ito, A. Nakajima, Characteristics of metal-oxide-semiconductor field-effect transistors with a functional gate using trap charging for ultralow power operation, *J. Vac. Sci. Technol. B* 31 (2013) 012206, <https://doi.org/10.1116/1.4773576>.
- [49] W. Zhou, X. Dai, T. Fu, C. Xie, J. Liu, C.M. Lieber, Long term stability of nanowire Nanoelectronics in physiological environments, *Nano Lett.* 14 (2014) 1614–1619, <https://doi.org/10.1021/nl500070h>.